A semi-empirical method for shear response modelling of masonry infilled frame structures

José Barros[a,c,*], Manuel Chiachío[b,c], Juan Fernández[b,c], Leandro Morillas[c], Joel Consuegra[a]

[a] *Faculty of Engineering, Catholic University of Santiago de Guayaquil, Guayaquil, Ecuador*
[b] *Andalusian Research Institute in Data Science and Computational Intelligence, University of Granada, 18071 Granada, Spain*
[c] *Dept. Structural Mechanics & Hydraulics Engineering, University of Granada, 18071 Granada, Spain*

Abstract

This paper presents a novel experimental and theoretical methodology for the fragility assessment of masonry infilled frame structures subjected to seismic loads. The method uses a Hamiltonian Monte Carlo Bayesian Neural Network trained with laboratory tests, to obtain the constitutive parameters of a non-linear spring model that represents the masonry shear behaviour. The resulting model accounts for several types of masonry units, structural steel and reinforced concrete frames along with the effects of windows and/or doors openings. The results show that the use of deterministic models lead to poor estimations about the in-plane behaviour of the system, whereas the application of the proposed semi-empirical method results in more robust predictions according to the measured data. Also, the proposed approach is tested against two extra data-sets to evaluate its extrapolation capabilities, with satisfactory results. Moreover, the proposed method has been applied to an engineering case study which demonstrates that it can be efficiently applied to robustly assess the safety against collapse of MIF buildings. Finally, a discussion between the proposed method and the current structural standards is provided within the context of the case study.

Keywords: masonry infilled frames, Bayesian Neural Networks, Hamiltonian Monte-Carlo, shear seismic response, Safety assessment.

1. Introduction

Structures made of masonry infilled frames (MIF) are one of the most widespread building structural systems around the world, because of their robust mechanical response, their insulation properties, waterproofing characteristics and low cost [41]. Figure 1 depicts a number of countries mentioned in damage reports from past seismic events, and where the MIF building system were used. However, there are no clear provisions on how to consider the actual contribution of the masonry infills within the structural safety of framed buildings.

*Corresponding author. E-mail: jose.barros@cu.ucsg.edu.ec

Indeed, the recent experience reported after seismic events (like the Pedernales' earthquake, Ecuador [19]), has demonstrated that the infilled frames can have both, positive and negative contribution to the seismic response, as shown in Figure 2. Such a disparity related with an aspect intrinsically connected with the risk of structural collapse, demonstrates the need for effective models to fairly consider the mechanical behaviour of these structural elements, and to understand its actual influence on the holistic seismic response of the buildings.

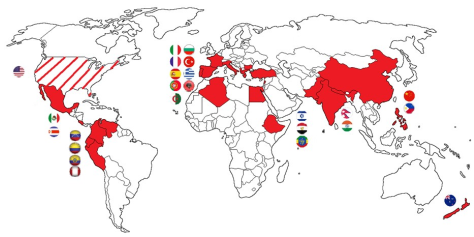

Figure 1: World map of seismic-prone countries with published reports of damaged masonry infilled frames: Barbosa et al. [4], Bennett et al. [8], Fierro et al. [22], Hak et al. [30], Irfanoglu [35], Kam et al. [39], Kaushik et al. [41], Maidiawati and Sanada [45], Perrone et al. [57], Tarque et al. [67], Urich and Beauperthuy [69], Villalobos et al. [71].

Figure 2: Example of dissimilar behaviour of masonry infilled frame structures after the Pedernales earthquake in Ecuador 16-04-2016 (courtesy of Eng. Raúl Hernández). Note that the building shown at the back of the picture revealed good performance, in contrast to the one at the front.

In the literature, a number of physics-based models have been proposed in the past years to replicate the behaviour of MIFs, and they can be typically classified as *micro*, *meso*, and *macro-models* [18, 50, 62, 67], according to their level of complexity. Micro and meso-modelling approaches are computationally expensive and require a big amount of input parameters about the infills and their disposition, which are typically not available and difficult to measure non-destructively. Therefore, they are not suitable for structural design nor for applications about evaluation of existing with MIF structures. Notwithstanding, these models can be used to enrich simpler models [60, 61], provided that enough information about the mechanical properties of the infills is available. On the other hand, macro-models rely on modelling the mechanical contribution of the masonry wall through a number of equivalent struts in the direction of each diagonal of the wall. The simplicity of this method makes it the one adopted by some structural codes, like the *Seismic Evaluation Standards* ASCE/SEI 41 [3]. Similar approaches can also be found in the recent literature about this topic [11, 34, 44, 49, 50, 52, 55]. Irrespectively, most of the referred methods in the literature exhibit a high variability in their results due to numerous sources of uncertainties, and consequently a lack of proper agreement when compared to experimental data [43, 44]. These sources of uncertainties are typically attributable to the lack of information about masonry and mortar strength-strain behaviour, joint interlock behaviour between different materials, and mechanical interaction between the frame and the wall, to cite but the most important. A recent work [20] has proposed a framework to assess the seismic performance of non-engineered constructed masonry infilled RC frame buildings, which considers the materials' uncertainties. Similar probabilistic approaches have been proposed recently [13, 42] for other types of structures and materials. Hence, the need and trend of the current research about this topic is heading towards the application of probabilistic approaches for the structural evaluation of existing MIF structures.

In this work, a novel semi-empirical framework to estimate the seismic response of masonry infilled framed structures with quantified uncertainty, is provided. The method uses a non-linear spring macro-model analogous to the macro-modelling approaches referred above, however, here the shear-response constitutive parameters of the non-linear spring are described through experimental probability distribution functions (PDFs). These PDFs are reproduced from Bayesian neural networks (BNN) trained using a data set comprising eighty five measured responses of a number of existing MIFs taken from the literature, and reproduced here under unified notation. Once trained, the BNN provides a probabilistic prediction of the shear wall behaviour, whereby to model the building seismic response with quantified uncertainty and to obtain its probability of collapse.

The BNNs has been chosen as data-driven method given the efficiency they have demonstrated in the quantification of the uncertainty [7, 10, 21]. Hamiltonian Monte Carlo [54] technique is adapted and used to train the BNN for its efficiency in dealing with high-dimensional models. The resulting neural network not only provides accurate mean predictions but also the range of plausible values, based on the amount of data available and their variability. In the literature, some approaches can be encountered which proposed the application of deterministic ANN to predict the behaviour of MIF [38]; however, using deterministic neural networks carries the disadvantage of ignoring about the quality of the prediction.

The proposed method has been compared against the models used by structural standards, including a variety of data-sets to evaluate its extrapolation capability, with satisfactory results. Finally, an engineering case study of a three-story building is presented to demonstrate its application to the level of an entire framed structure. This case study is based on the work by Morandi et al. [51], and more precisely, based on its laboratory test results, as a basis for comparatively evaluate structural behaviour and safety assessment capabilities of the proposed approach.

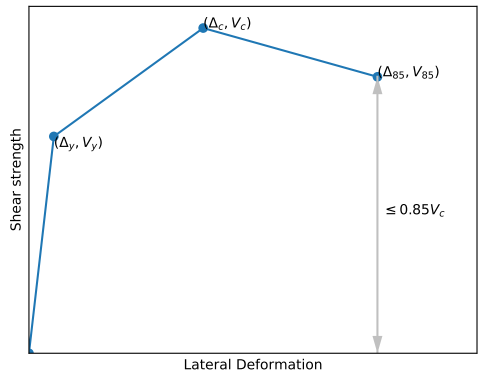

Figure 3: Shear behaviour of a masonry infilled frame. The pairs (Δ, V) indicate the coordinates of lateral deformation (Δ) and shear (V) at key indicative points, namely yielding (Δ_y, V_y), capping (Δ_c, V_c), and residual point (Δ_{85}, V_{85}).

The rest of the paper is structured as follows. Section 2 presents the foundations of the mechanical modelling of MIF under an unified notation. Section 3 describes the prediction of the masonry wall constitutive parameters through the HMC-BNN method, which has been made available for the readers trough a permanent link. A comparison of the HMC-BNN results with the estimations of the models currently found in the literature, is presented in Section 4. Section 5 describes and discusses the engineering case study, and finally section 6 gives concluding remarks.

2. Empirical mechanical description of MIFs

In this section, the strategy adopted to experimentally characterize the shear behaviour of the MIF structural system is presented. To this end, a database of eighty five laboratory test available in the literature are used as input data to train and test the BNN model. These tests consist of one-bay and one-story MIFs, subjected only to in-plane lateral cyclic deformation. Table 1 provides an overview of the data set considered with specification of the type of frame, masonry unit, amount of tests of each reference and presence of wall-openings. Additional information about the test can be found in Tables 7, 8 and 9 in the Appendix. Note that the results of shaking table tests available in the literature (such as [37, 58, 66]) provide very important information for better understand the MIF structural system; however, they have not been used in the present work due to the difficulty in defining the constitutive behaviour of the system given the degradation effects to which they are subjected during the typical testing protocols.

Figure 4 shows distributions of the descriptive parameters of the MIF within the database. These parameters are the masonry unit type, failure type observed, height-to-thickness ratio, and a frame-infill stiffness relation, originally proposed by Stafford Smith and Carter [65], also referred to as λ, which is given as follows:

$$\lambda = \sqrt[4]{\frac{E_m t_m \sin 2\gamma}{4E_c I_c h_m}} \tag{1}$$

Table 1: Database of experimental tests.

Reference	No. of tests	Frame	Masonry	Tests with openings
Flanagan and Bennett [23]	13	Steel	Horizontal hollow clay brick	1
Markulak et al. [47]	5	Steel	AAC and hollow clay bricks	0
Schneider et al. [63]	5	Steel	Solid clay bricks	5
Tasnimi and Mohebkhah [68]	5	Steel	Solid clay bricks	4
Morandi et al. [51]	4	RC	Hollow clay bricks	1
Basha and Kaushik [5]	6	RC	Fly ash bricks	0
Calvi et al. [12]	7	RC	Hollow clay bricks	0
Gazić and Sigmund [25]	9	RC	Solid and hollow clay bricks	0
Guerrero et al. [28]	3	RC	Hollow concrete bricks	0
Haider [29]	4	RC	Solid clay bricks	0
Jiang et al. [36]	6	RC	AAC	0
Mansouri et al. [46]	4	RC	Solid clay bricks	3
Mehrabi et al. [48]	6	RC	Solid and hollow concrete bricks	0
Sigmund and Penava [64]	8	RC	Hollow clay bricks	8

In the last equation I_c is the second moment of area of the frame's columns cross section, whereas E_m and E_c are the Young's moduli of the infill and frame, respectively. The terms t_m, h_m and γ, are the thickness, height and the slope of the representative diagonal of the infill, respectively.

3. Data-based modelling of infilled masonry walls constitutive parameters

This section provides a data-based model to obtain the constitutive parameters of a MIF (depicted in Figure 3), using the data explained in Section 2 and given in the Appendix. As indicated before, the model consists of a one-dimensional non-linear shear spring with a tri-linear constitutive behaviour (see Figure 3), which represents the shear response of the frame and wall system as a whole. Here, the referred constitutive parameters of the model are established through a BNN, presented next.

3.1. Hamiltonian Monte Carlo based-Bayesian Neural Networks

As previously stated, identifying the degree of belief in the predictions made by any model is of great importance [26] and can be critical in the subsequent decision-making stage. Thus, BNN have been chosen as the data-driven method.

Among the state-of-the-art training algorithms for BNN, the Hamiltonian Monte Carlo (HMC) method [53], a variant of Markov Chain Monte Carlo (MCMC) [27, 54], is gaining importance and seems to be the gold standard nowadays [7]. As other Bayesian training algorithms, HMC aims to find an approximation of the posterior distribution $p\left(\theta|\mathcal{D},\mathcal{M}\right)$ by sampling from a Markov Chain, where $\theta = \{w,b\} \in \Theta \subseteq \mathbb{R}^d$ represents the weights (w) and biases (b) of the BNN, $\mathcal{D}$ the data, and $\mathcal{M}$ the model class, which in this case is related to the BNN architecture.

The Hamiltonian method, in a context of conservative dynamics, is built on the premise that volumes are preserved. Every particle is defined by its position and momentum, and as a consequence, any change in the

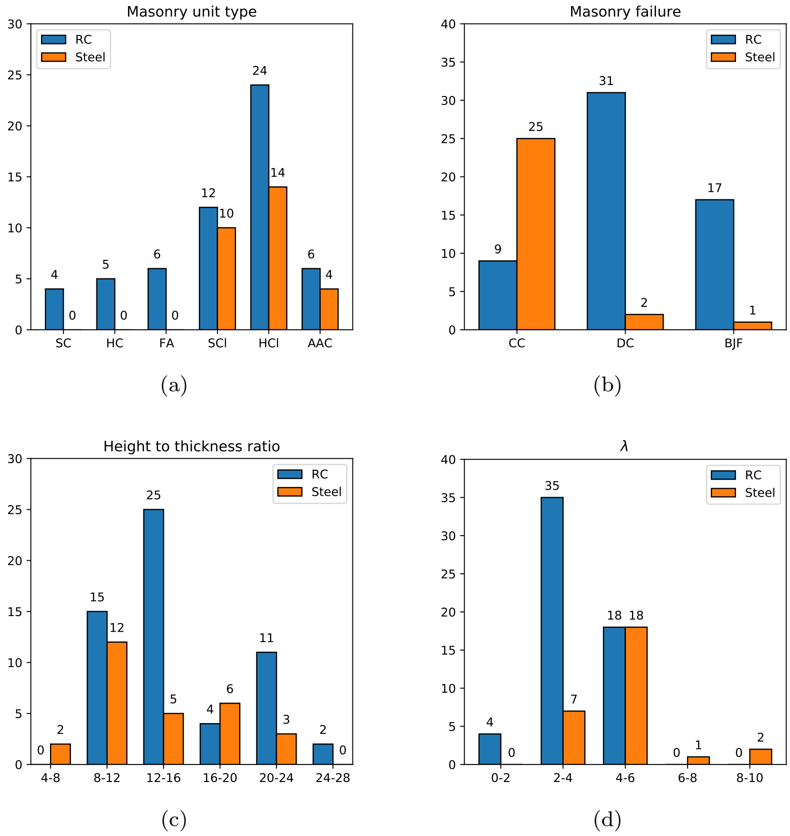

Figure 4: Distribution of the following parameters within the database: (a) Masonry unit type, (b) Masonry failure observed, (c) Height to thickness ratio, (d) λ parameter. SC: Solid Concrete, HC: Hollow Concrete, FA: Fly Ash, SCl: Solid Clay, HCl: Hollow Clay, AAC: Autoclaved Aerated Concrete; CC: Corner Crushing, DC: Diagonal Cracking, BJF: Bed-Joint Failure.

position space needs to be compensated with a change in the momentum space, so that the position-momentum phase space is maintained. In the Hamiltonian Monte Carlo context [9], the position space is replaced by the parameter space, and an auxiliary momentum variable p is adopted, hence any parameter value θ is associated with a momentum leading to the pair (θ, p). Once the momentum variable has been included and the parameter space converted to a phase space, namely $\theta \to (\theta, p)$, a joint probability distribution, namely the canonical distribution is defined as follows:

$$\pi(\theta, p) = \pi\left(\theta|q\right)\pi(q) = e^{-H(\theta,p)} \tag{2}$$

where $H(\theta, p)$ is the Hamiltonian function, also called as the energy at that point, and can be expressed as:

$$H(\theta, p) = -\log \pi(\theta, p) = -\log \pi\left(\theta|q\right) - \log \pi(\theta) \tag{3}$$

with $\pi\left(\theta|q\right)$ often assumed a Gaussian distribution $\mathcal{N}\left(p|0, M\right)$ with covariance matrix (also known as mass matrix) M, and $p \sim \mathcal{N}(0, I)$.

In this method, new samples θ_n are drawn using the *leapfrog integrator* [9], with a step size ϵ and a path length L, as depicted in Algorithm 1. These samples are then accepted with probability α, as per Equation 4.

Algorithm 1 *Leapfrog Integrator*

```
Obtain initial samples θ_0 ← θ and p_0 ← p
for 0 ≤ n < L/ε do
    p_{n+1/2} ← p_n − (ε/2)(dV/dθ)(θ_n)
    θ_{n+1} ← θ_n + ε p_{n+1/2}
    p_{n+1} ← p_{n+1/2} − (ε/2)(dV/dθ)(θ_{n+1})
end for
```

$$\begin{aligned} \alpha &= min\left(1, \frac{\pi(\theta_{n+1}, -p_{n+1})}{\pi(\theta_n, p_n)}\right) \\ &= min\left(1, \frac{\exp(-H(\theta_{n+1}, -p_{n+1}))}{\exp(-H(\theta_n, p_n))}\right) \end{aligned} \tag{4}$$

The HMC algorithm is very sensitive to small variations in the step size and path length hyperparameters, thus finding the right values is a critical aspect of this method. The open source software *hamiltorch*[1] has been used in this paper for the implementation of the HMC algorithm. The hyperparameters have been chosen as follows; step size $\varepsilon = 0.001$, leapfrog steps $L = 10$, the prior PDFs of θ, namely, $p(\theta)$, are chosen as Gaussian with prior precision for the parameters $\tau = 1$, likelihood output precision $\tau_{out} = 100$ and 500 samples where 250 are burned. The chosen activation function for the hidden layers is the Rectified Linear Unit, *ReLu*, and the activation function for the output layer is the *Sigmoid*. The HMC-BNN model consists of one input layer with six neurons, two hidden layers with 40 neurons each, and one neuron output layer, making a total of 1961 parameters to be learned for each constitutive value. A ReLU activation function is assigned to the neurons of the hidden layers, whilst a Sigmoid function is applied to the neuron in the output layer, as indicated in the previous section

3.2. Training of the HMC-BNN with experimental data

Here the experimental database presented in Section 2 is employed to train the HMC-BNN which, as already stated above, will act as data-based model to estimate the constitutive parameters of MIFs in a probabilistic fashion. Note that, due to the limited amount of data, it was decided that the proposed data-based model consists of an uniaxial shear spring representing the overall behaviour of the in plane frame-wall system.

To this end, the six-neurons input layer of the HMC-BNN is defined to account for the following input parameters (for clarity, some of those parameters have been represented in Figure 5):

[1] https://github.com/AdamCobb/hamiltorch

- Height to thickness ratio (h_m/t_m). According to [2], this parameter has a direct influence on the peak lateral strength in the plane of the wall.

- Height to length ratio (h_m/L_m). As this parameter is related to the dimensions of the infill, it has a direct impact on the stiffness, as others have observed [34, 59].

- λ parameter (see Equation (1)). This parameter has been widely used for MIF characterization [18, 50, 67], as it relates the stiffness of the infill to the stiffness of the frame and, indirectly, to their respective strengths. It can be used to estimate whether the wall or the frame will govern the stiffness and strength of the system.

- Axial load to strength ratio ($P/A_m f_m$). The behaviour of masonry can be predicted with shear-friction models [15] and, therefore, the influence of axial load has a fundamental influence in the estimation of the strength and deformation capacity of the system.

- Ratio of net infill strut area (A_{is}/A_s). The net infill strut area A_{is} is considered as the masonry area within the equivalent strut width w_m [33] accounting for the openings, whilst the gross infill strut area, A_s, is the area within the equivalent strut width, without considering the openings. w_m is obtained as one third of the length of the wall diagonal (d_m, as indicated in Figure 5). Several equations have been proposed in the literature to estimate the equivalent strut width; however, the authors chose to use the equation with the largest width to provide an adequate characterization of the wall openings. This parameter, which is normalized to the gross area of the masonry wall, allows us to consider the presence of openings in the wall, including a way to differentiate the asymmetric cases.

- Masonry unit type. It is known that the different materials used to fabricate masonry units and whether they are made solid or hollow, result in important differences in their behaviour [2, 14].

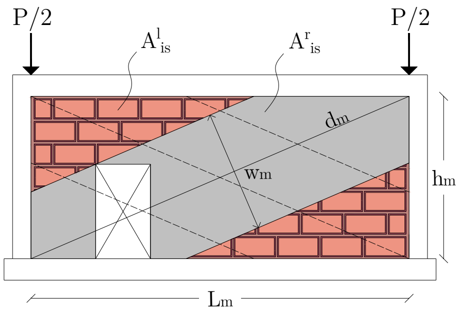

Figure 5: Illustration of the geometric parameters used in the MIF dataset.

Correspondingly, the output layer accounts for the point of first stiffness drop (Δ_y, V_y), capping point (Δ_c, V_c) and residual strength (Δ_{85}, V_{85}) pairs of lateral deformations and shear forces (recall Figure 3). Here, the capping point is defined as the Δ, V pair of the maximum strength of the envelope line of the test. The first stiffness drop corresponds to the intersection of the elastic part of a bi-linear approximation with the envelope curve of the test (similar to a yield point for ductile structural systems), whereas, the residual is the point within the envelope behaviour that is lower or equal to the 85$^{\text{th}}$ percent of the maximum strength.

Once trained, the HMC-BNN provides a probabilistic prediction of the three constitutive (Δ, V) pairs of a MIF, where specific geometrical and mechanical parameters act as inputs to the BNN. Figure 6 shows the prediction results of the trained HMC-BNN for a hollow concrete masonry infilled concrete frame with 300x300 [mm] columns. The results were obtained using the following inputs: $h_m = L_m = 3000$ [mm], $t_m = 100$ [mm], $f_m = 10$ [MPa], $E_m = 9$ [GPa], $f_c = 20MPa$, and $E_c = 21.0$ [GPa]. Note that the prediction denotes the high level of uncertainty that affects this structural system. Also, observe that the quantified uncertainty provided by the proposed method enables us to perform a probability safety assessment of the MIF structures with no extra difficulties. To ease the practical application of the method, and for the sake of reproducibility, the reader can find the trained neural network for direct application at `https://github.com/josebarroscabezas/MIF-HMC-BNN`.

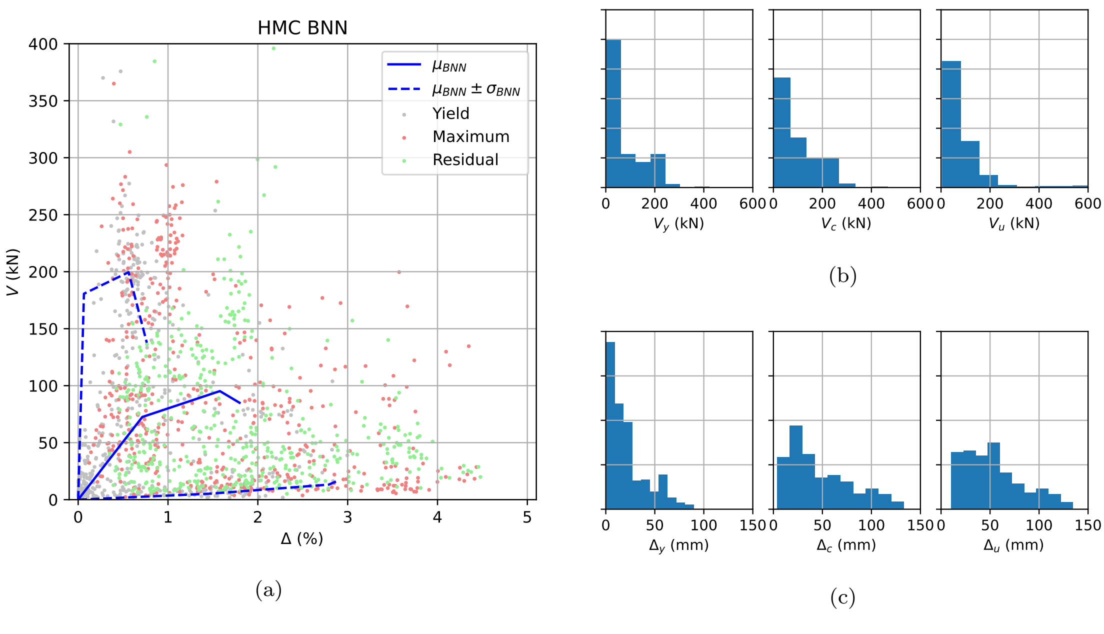

Figure 6: Prediction results of the shear-response constitutive parameters using the HMC-BNN method. Panel (a): Predicted constitutive (V, Δ) pairs. Panels(b) and (c): distribution of the characteristic shear and lateral deformation values of the tri-lineal approximation, respectively.

4. Comparative analysis using existing models

In this section, the prediction capabilities of the proposed method are analysed and also discussed with respect to models available in the literature. The frame and masonry strut modelling approaches are briefly presented, followed by a comparison of their results against to the proposed method herein.

4.1. Frame models used for comparison

To physically model the shear behaviour of the MIF structural system, the framework *OpenSeespy* [72] is used, where a macro-modelling approach with a single strut per diagonal is applied according to three different models proposed by other researchers in Liberatore et al. [44], Huang et al. [34] and ASCE/SEI 41 [3]. For the concrete frame, where applicable, the beam and columns are modelled using the recommendations by Haselton et al. [32]; otherwise, a fiber section within a non linear beam column element, with a force-based formulation, is applied. Two different approaches are adopted to represent the behaviour of the reinforced concrete frames, namely: (1) models with concentrated hinges at the ends of beam-column elastic elements, following the recommendations by Haselton et al. [32]; and (2) models based on beam-column elements with distributed plasticity. Table 2 shows the general formulation to obtain the constitutive parameters of the nonlinear hinges, whereas Figure 7a depicts the general geometry and characteristics of the model. Notice that the second approach is also used in Liberatore et al. [44], where the concrete and steel constitutive uni-axial behaviour is discretized within the cross section, to be further integrated over the length of the beam column element. This allows us to directly consider the distribution of plasticity along the element. A similar approach was applied to model the steel frames. Additionally, Table 3 and Figure 7b show the general geometry and characteristics of the model. The shear behaviour of the columns is not explicitly modelled since the tests within the database do not include cases with that type of failure.

Table 2: Description of constitutive values for a structural model of reinforced concrete using non-linear concentrated hinges.

Description of constitutive parameters
$k_o = 1.1\dfrac{11EI_{40}}{L_v}$ $EI_{40} = \left[-0.02 + \dfrac{0.98P}{A_g f_c} + 0.09\dfrac{L_v}{H}\right] E_c I_g$ M_y (according to Panagiotakos and Fardis [56]) $M_c = 1.25\,(0.89)^{\frac{P}{A_g f_c}}\,(0.91)^{0.01 f_c}\,M_y$ $\phi_c = \phi_y + 0.12\,(1.55)\,(0.16)^{\frac{P}{A_g f_c}}\,(0.02 + 40\rho_{sh})^{0.43}\,(0.54)^{0.01 f_c}\,(0.66)^{0.1 s_n}\,(2.27)^{10\rho}\,F_{SYM}$ $\phi_r = \phi_c + 0.76\,(0.031)^{\frac{P}{A_g f_c}}\,(0.02 + 40\rho_{sh})^{1.02}$

Formulation of non-linear hinges according to Haselton et al. [32], in units of N, mm and MPa. L_v: shear length, P: axial load, A_g: gross area of the cross section, f_c: concrete characteristic compressive strength, H: height of the cross section, ρ_{sh}: transverse steel ratio, s_n: rebar buckling coefficient according to Dhakal and Maekawa [17], ρ: ratio of tension reinforcement, F_{SYM}: factor to consider asymmetric arrangement of flexural reinforcement. Greek letter ϕ is used here to denote a rotation.

4.2. Masonry strut models used for comparison

Three different models were adopted to estimate the constitutive behaviour of the masonry's equivalent strut. *Pinching4* constitutive behaviour is used herein to construct the model. For the ease of the reader, the formulation of these models are summarized in Table 4 under a unified notation. The shapes of their

Table 3: Description of constitutive values for a structural model of reinforced concrete using uniaxial distributed plasticity.

	Concrete	Steel
Peak/Yield stress	f_c	f_y
Peak/Yield strain	$\epsilon_o = \dfrac{105 + f_c}{70000}$	$\epsilon_y = \dfrac{f_y}{E_s}$
Ultimate stress	12	
Ultimate strain	$5\epsilon_o$	
Strain hardening ratio		$\beta = 0.001$
OpenSeespy model	*Concrete01*	*Steel02*

Parameter formulation according to Karthik and Mander [40], in units of N, mm and MPa. Recommended values of $R_0 = 18$, $CR_1 = 0.912$ and $CR_2 = 0.15$, of Steel02 model, were adopted.

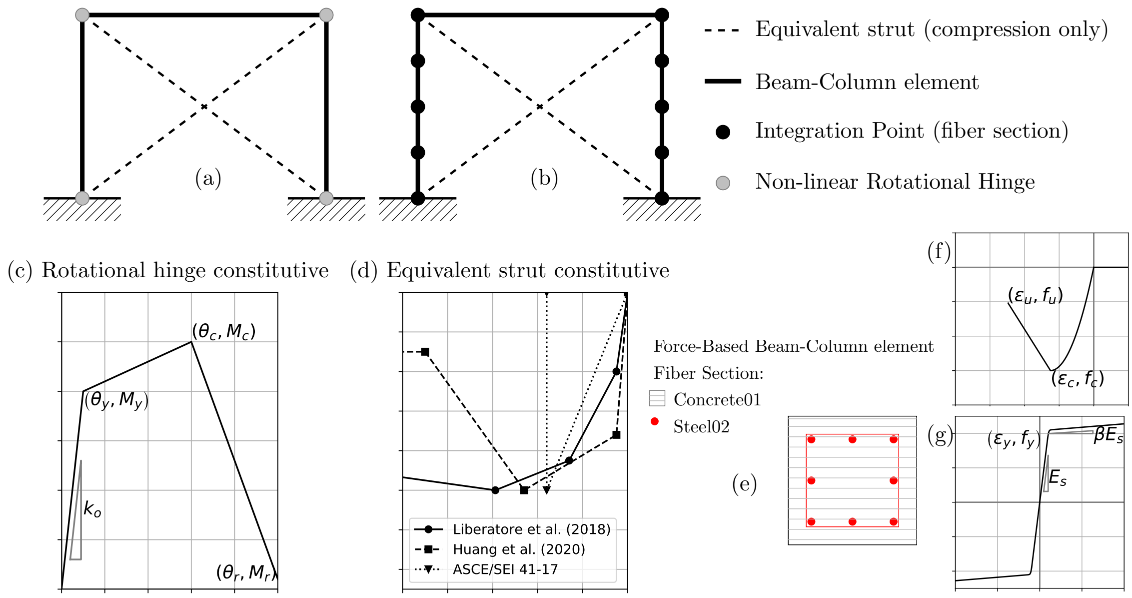

Figure 7: Models used for comparison in Section 4. (a) Frame model with concentrated hinges at the ends of beam-column elements, with a (c) tri-lineal constitutive behaviour. (b) Frame model with distributed plasticity beam-column elements, with a (e) fiber section discretized with uniaxial stress-strain behaviour of (f) concrete and (g) steel. (d) Equivalent strut shear-deformation behaviour.

constitutive behaviour are given in Figure 7d. The first model, proposed in Liberatore et al. [44], consists of a 4-lines backbone curve where the strength is estimated according to four possible failure modes, namely: bed-joint sliding, diagonal tension, diagonal compression, and corner compression. The formulation of the failure modes are adapted from Decanini and Fantin [16], and corrected by a regression study using the laboratory test data of this work.

The second strut model, proposed in Huang et al. [34], also consists of a 4-lines backbone curve; however, the characteristic strength and deformation values were obtained by a multivariate regression analysis. Finally, the third strut model, proposed in ASCE/SEI 41 [3], consists of a 2-line backbone curve, as shown in Figure 7d.

Table 4: Description of the constitutive parameters for the three masonry strut models used for comparison.

	Liberatore et al. [44]	Huang et al. [34]	ASCE/SEI 41 [3]
Strength at 1$^{\text{st}}$ stiffness drop	$0.40V_p$	$0.72F_c$	-
Strength at 2$^{\text{nd}}$ stiffness drop	$0.85V_p$	-	-
Maximum strength	$V_p^{(1)}$	F_c	$V_P^{(2)}$
Residual strength	0	$0.40F_c$	0
Deformation at 1$^{\text{st}}$ stiffness drop	$0.00025H_m$	$\dfrac{0.72F_c}{K_e}$	
Deformation at 2$^{\text{nd}}$ stiffness drop	$0.0013H_m$	-	
Deformation at maximum strength	$0.00294H_m$	δ_c	$\min\left(\dfrac{V_P}{K_m}, \delta_r\right)$
Maximum deformation	$0.0344H_m$	$\dfrac{0.60F_c}{K_{pc}} + \delta_c$	

E_m, f_m: elastic modulus and masonry characteristic compressive strength, respectively. t_m: thickness of the wall, l_d, ϕ: length and direction of the diagonal of the wall, respectively. H_m, L_m: wall height and length, respectively.
$V_s = [(1.2\sin\phi + 0.45\cos\phi)\,\tau_0 + 0.3\sigma_y]\,t_m L_m$: bed-joint sliding failure mode; $V_{dt} = (0.6\tau_{m0} + 0.3\sigma_y)\,t_m L_m$: diagonal tension failure mode; $V_{dc} = 1.16\tan\phi\,(\lambda_h)^{-1} f_m t_m L_m$: diagonal compression failure mode; $V_{cc} = 1.12\sin\phi\cos\phi\lambda_h^{-0.88} f_m t_m L_m$: corner compression failure mode. τ_0: bed joints basic shear strength, τ_{m0}: shear strength from diagonal compression test, σ_y: vertical stress, λ_h: Stafford-Smith coefficient (see Equation (1)). $K_e = 0.0143E_m^{0.618} t_m^{0.694} H_m^{-1.096} L_m^{1.096}$: initial stiffness of the compressive strut, according to strut model 2. $K_{pc} = -1.278 f_m^{-0.357} t_m^{-0.517} K_e$: post-capping stiffness, according to strut model 2. $K_m = 1/\left(k_f^{-1} + k_s^{-1}\right)$: stiffness of the MIF system as a serial combination of frame stiffness (k_f) and shear wall stiffness (k_s). δ_r: residual deformation as a function of columns shear strength and stiffness and wall shear strength and stiffness, according to ASCE/SEI 41 [3]. $V_p^{(1)} = 0.98\min(V_s, V_{dt}, V_{dc}, V_{cc})$, $F_c = 0.003766 f_m^{0.196} t_m^{0.867} l_d^{0.792}$, $V_P^{(2)} = 0.33 f_m H_m t_m$.
$\delta_c = 0.0154E_m^{-0.197} H_m^{0.978} L_m^{-0.978}$

4.3. Comparative results using data within the training database

Using the modelling approaches presented in Sections 4.1 and 4.2, four MIF models are constructed and further compared to the proposed approach presented in Section 3. The aforementioned models are briefly identified as follows:

- Model 1: Concentrated hinges frame model with a quadri-linear constitutive equivalent strut [44];
- Model 2 :Concentrated hinges frame model with a tri-linear equivalent strut [34];
- Model 3: Fiber section based frame model with the same equivalent strut of the first model;
- Model 4: Fiber section based frame model with a bi-linear constitutive equivalent strut [3].

In this comparative analysis, the results of the proposed BNN model are represented by its mean response and also by the scatter plots of the predicted values of (V, Δ) points. Recall that the proposed model is only a one-dimensional shear spring and does not consider the separate behaviour of the frame and the infill as usual in macro-models.

Figures 8 to 11 show the comparative results between the proposed model and the four models used for comparison, along with representation of the laboratory data used as reference. All tests correspond to reinforced concrete fully infilled frames, where solid clay, hollow clay, solid cement and hollow cement masonry units were used, respectively. From these results, the following remarks can be highlighted:

- Model 1 correctly estimates the initial stiffness and maximum strength of the system in the case of solid clay MIF. However, note that the model is not capable to capture the mechanical response after the degradation of the structure. For the cases of solid cement, hollow clay and hollow cement units MIF, the model under-predicts the initial stiffness and is not capable to capture the degradation of the system.

- Model 2 correctly captures the initial stiffness of the MIF with solid clay, solid cement and hollow cement units. However, the model over-predicts the strength of the system for solid and hollow clay units MIF, and under-predicts the strength of solid and hollow cement units MIF. In all cases, the model does not capture the mechanical response after the degradation.

- Model 3 correctly estimates the initial stiffness and maximum strength of the system with solid clay units; although, it is not capable of capturing the degradation of the structure. In the case of hollow clay units, the initial stiffness is under-predicted, whilst the maximum strength and deformation capacity is over-predicted. Finally, for the cases of solid and hollow cement units, the model under-predicts the initial stiffness and maximum strength, and does not capture the degradation of the system.

- Model 4, under-predicts in all cases the initial stiffness and maximum strength, over-predicts the deformation capacity, and does not capture the mechanical response after degradation.

- Observe that the proposed HMC-BNN model correctly predicts the initial stiffness of the system in average, for the cases of the usage of solid clay, solid cement and hollow cement units, and only under-predicts the initial stiffness of the system when hollow clay units are used. For all cases, the maximum strength result of each test is enclosed by the set of values that conform the prediction of the proposed model. In general, the HMC-BNN mean model does not properly capture the deformation capacity of the system.

In general, the previous observations indicate that the level and sources of uncertainties of the MIF structural system should be considered when performing a structural evaluation of a building, since none of the available deterministic models can capture all of the properties of the lateral response of the system for all of the masonry unit types. On the other hand, the scatter points obtained after simulating our proposed BNN model, presented in Figures 8 to 11, clearly capture all of the characteristics of the lateral response of the system within the prediction range. As also mentioned in Liberatore et al. [44], this uncertainty should be accounted for to properly evaluate an existing structure.

Figure 12 shows the measured results from a laboratory test for a case with steel frame with hollow clay masonry units. The results of the proposed BNN model are drawn along with the prediction of models 3 and 4. Model 2 was adapted by using the fiber section approach to model the behaviour of the frame. As can be seen, models 2 and 3 over predict the maximum strength and the initial stiffness of the system and do not

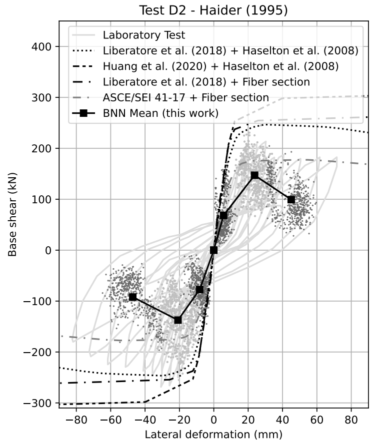

Figure 8: Comparative results obtained for solid clay masonry infilled reinforced concrete frames.

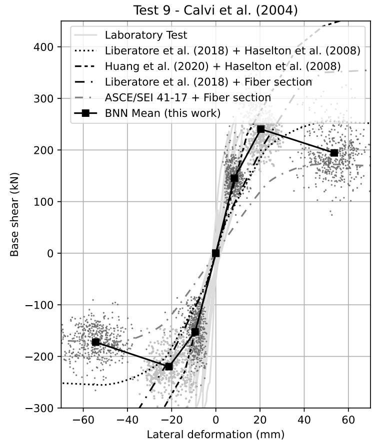

Figure 9: Comparative results obtained for hollow clay masonry infilled reinforced concrete frames.

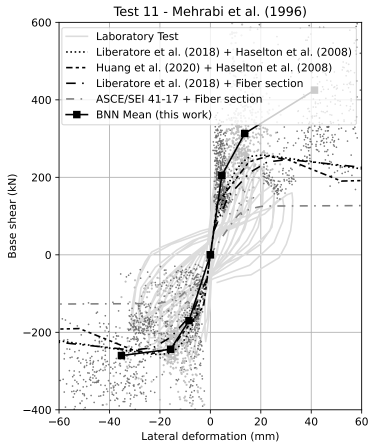

Figure 10: Comparative results obtained for solid cement masonry infilled reinforced concrete frames.

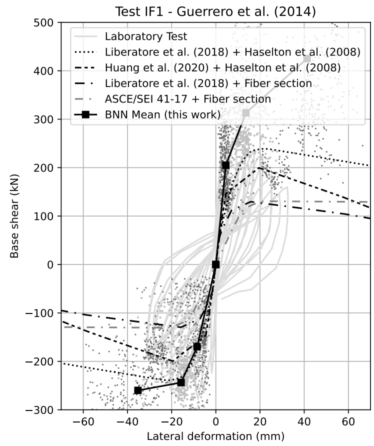

Figure 11: Comparative results obtained for hollow cement masonry infilled reinforced concrete frames.

properly capture the degradation of the structure. Model 4, on the other hand, fairly predicts the initial stiffness and maximum strength of the system, however it also fails to reproduce the degradation. The BNN mean model properly captures the maximum strength and degradation of the mechanical system, although it over-predicts the initial stiffness.

Besides, Figure 13 shows the measured results from a laboratory test of a steel frame with hollow clay units with a non-symmetric window opening located at the upper corner of the wall. Only the model 4 can account for the reduced strength of the system due to the presence of the opening. Accordingly, only the prediction of that model is compared to the proposed BNN model. Clearly, model 4 does not properly captures the behaviour of the system. Observe that the BNN mean model also over-predicts the initial stiffness and strength of the wall and does not properly captures the degradation. Notwithstanding, the

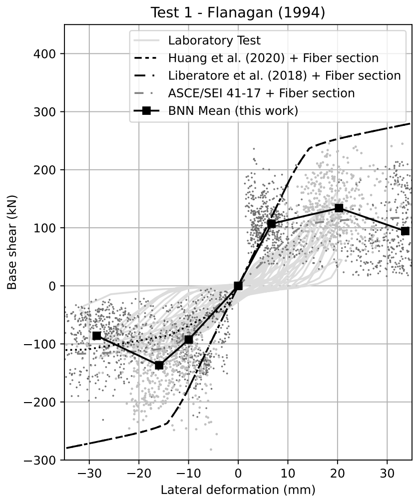

Figure 12: Comparative results obtained for hollow clay masonry infilled steel frames.

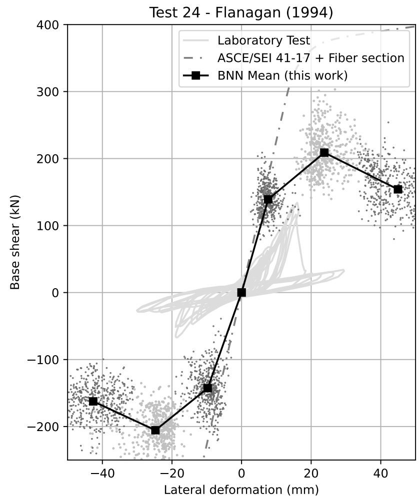

Figure 13: Comparative results obtained for hollow clay masonry infilled steel frames with a window opening.

result is better than the available model of the literature.

Notice that the experimental tests shown in Figures 9 to 13 were part of the training set of the BNN, whilst the one in Figure 8 was part of the test set of the BNN. Figure 14 compares the prediction of the proposed BNN model with the force results of the first steel and concrete MIF tests from the database, showing that the probabilistic prediction of the model provides a valid envelope (represented using grey lines) of the expected real result. These results demonstrate the capabilities of the proposed BNN model to be applied on the structural probabilistic evaluation of the lateral strength of MIF existing buildings.

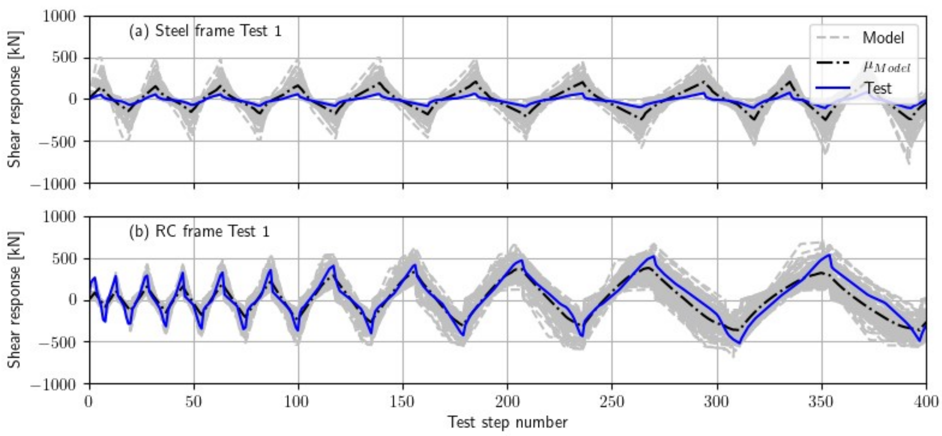

Figure 14: Results of the proposed model predictions in comparison to real tests used as reference. Panel (a): a masonry infilled steel frame tested by Flanagan and Bennett (1999); panel (b): masonry infilled concrete frame tested by Morandi et al. (2018a).

In the following section, the extrapolation capabilities of the model is further discussed.

4.4. Analysis of extrapolation capability

In this section, experimental test out from the database presented in Section 3 were selected to evaluate the prediction capabilities of the proposed method. Table 5 summarises information from four experimental tests available in the literature: one full-scale static test and three shaking table tests at different scales.

The experimental test performed by Furtado et al. [24], corresponds to a full-scale cyclic in-plane loading test of a double-leaf MIF with hollow clay units. The wall was composed by a 150 mm thick external leaf, and a 110 mm thick internal leaf, with a gap of 40 mm between the leafs. Notice that the database does not consider any case of double-leaf MIF, however, the prediction was made assuming an input thickness of the masonry wall equal to the sum of the leafs of the tested system. Figure 15 shows the BNN mean model prediction against the laboratory test results. As can be seen, the proposed model prediction of the strength of the system is appropriate. Unfortunately, the test was stopped until the specimen reached 0.5% drift, so it can not be compared for higher deformations.

The results of the experimental test performed by Benavent-Climent et al. [6], are compared to those predicted by the proposed BNN model. According to the authors, the reinforced concrete frame was part of eleven previous seismic simulations before the masonry wall was built and, therefore, some level of degradation of the columns was expected (the authors report 1.5% maximum inter-story drift and 0.12% of residual inter-story drift). Therefore, instead of using the gross inertia as an input to the BNN model, a cracked section was used assuming 30% of the gross section as effective. The masonry infill was tested as a retrofit system. As shown in Figure 16, the proposed model over-predicts in average the maximum strength, however the scatter points capture the overall behaviour of the test.

The third and fourth tests presented in Table 5 (i.e. Kallioras et al. [37] and Stavridis et al. [66]), were also compared to the proposed BNN model prediction. As can be seen in Figures 17 and 18, an acceptable prediction is observed in terms of strength; however, the proposed model overestimates the deformation capacity of the system. Irrespectively, note that the proposed model presents a sufficiently wide range to contain the measured value within the predicted result, both in terms of deformation as well as strength.

Table 5: Relevant information of experimental tests available in the literature (Units in MPa, mm and kN)

Reference	λ [%]	f'_m	E_m	t_m	h_m	L_m	Unit type	P	A_{is}/A_s
[24]	0.192	13.4	9420	260	2300	4200	Hollow Clay	270	1.00
[6]	0.305	10.0	6600	40	1400	2000	Hollow Clay	60	1.00
[37]	0.101	4.7	2300	75	3000	4000	Hollow Clay	25	1.00 / 0.80
	0.114	4.7	2300	120	3000	4000	Hollow Clay	25	1.00 / 0.80
[66]	0.170	19.8	5410	120	2240	3660	Solid Clay	-	1.00 / 0.85

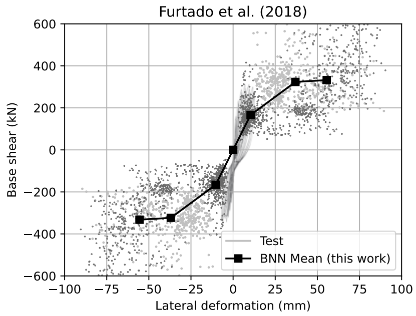

Figure 15: Results obtained for static test on hollow clay double-leaf masonry infilled concrete frame.

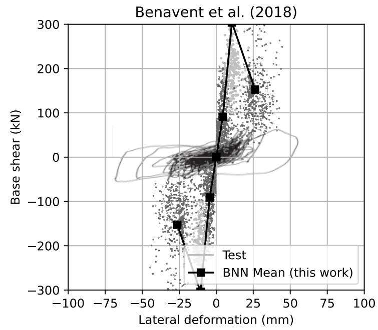

Figure 16: Results obtained for hollow clay masonry infilled concrete frame previously subjected to lateral deformation.

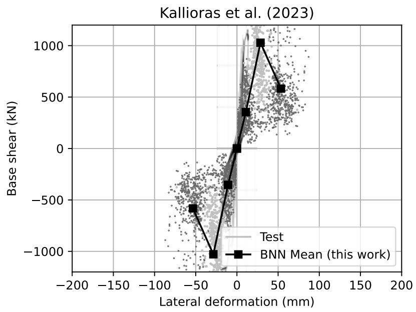

Figure 17: Results obtained for a two bay hollow clay and a two bay double-leaf hollow clay masonry infilled concrete frame previously subjected to several seismic records. One bay of each kind of wall had a door opening.

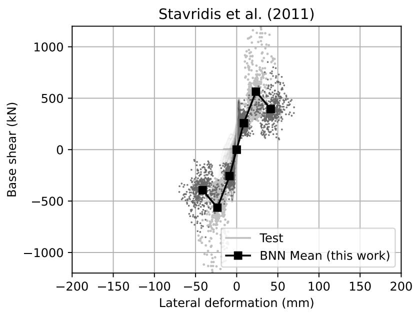

Figure 18: Results obtained for a two bay solid clay double-leaf masonry infilled concrete frame previously subjected to several seismic records. One bay had a window opening.

5. Engineering case study

In this section, the proposed model is used to evaluate the seismic collapse probability of a three story MIF building. Results are compared to a code-based evaluation with the ASCE/SEI 41 [1], and also using the model proposed by Huang et al. [34]. The aforementioned building has been selected to match the properties of a one-bay and one-story laboratory test by Morandi et al. [51], whose geometrical and mechanical characteristics are given in Table 6. The building is considered as 14x14 [m] plan with two MIF as lateral resisting structure, with 3.30 [m] floor height. The total mass of each floor is estimated as 62000 [kg].

In this study, the seismic collapse probability is estimated by means of non-linear time history analyses

Table 6: Geometrical and mechanical parameters of the MIF used for the case study.

	Value	**Unit**		**Value**	**Unit**
L_m	4220	[mm]	ρ_{col}	2.48	%
H_m	2950	[mm]	ρ_{beam}	0.47	%
t_m	350	[mm]	f'_c	34.0	[MPa]
b_{col}	350	[mm]	f_y	521.0	[MPa]
b_{beam}	350	[mm]	f'_m	4.60	[MPa]
h_{beam}	350	[mm]	E_m	5299	[MPa]

using far-field records data set of the FEMA P-695 document [31]. Normalization and scaling of the seismic records are taken from Table A-3 of the aforementioned document. The proposed 2D data-based model consists of three sets of three in-parallel springs connected in series to three equal masses. The model was constructed in Openseespy platform [72], using the *hysteretic* material as constitutive behaviour. For comparison purposes, the model proposed by Huang et al. [34] (see Section 4) is applied both with a blind prediction and after a calibration with the test results. In the next section, a discussion about the estimation of the natural period of the structure is presented.

5.1. Fundamental period estimation

According to ASCE/SEI 41 [1] provisions, and particularly to its equation 12.8-9 (reproduced here for ease of the reader), a lower bound estimation of the MIF fundamental period can be obtained as:

$$T_a = \frac{C_q}{\sqrt{C_w}} h_n = \frac{0.0058 h_n}{\frac{1}{A_B} \sum_{i=1}^{x} \frac{A_i}{\left[1 + 0.83\left(\frac{h_n}{D_i}\right)^2\right]}} \tag{5}$$

where A_B is the area of the base of the structure in m^2, x is the number of shear walls in the direction under consideration, A_i and D_i are the web area (in m^2) and the length of shear wall i (in m), respectively, and h_n is the structural height of the building in m, resulting $T_a = 0.32$ [s].

Considering that most these factors are subjected to much uncertainties (i.e. epistemic uncertainties in the the mass and stiffness of the structure, those related to soil stiffness, soil-structure interaction and relative deformations in wall-frame joints, among others), the fundamental period predictions obtained from the deterministic models hardly match with the period measured in a real case structure. Thus, our proposed method is used here to obtain that measure with quantified uncertainty and the results are given in Figure 19. These results show that the most likely period for our case study structure is around 0.30 to 0.40 seconds. Note that the blind and calibrated predictions of the fundamental period using [34], are also given, and resulted in $T_d = 0.091$ [s] and $T_{dm} = 0.11$ [s], respectively. Note also that the result of Equation (5) lays within the range of most probable fundamental period estimated from our proposed model. Our results also are in agreement with those obtained for a three story building, which was evaluated by Varum et al. [70] after Ghorka 2015 earthquake. In such study, ambient vibration test were performed to identify the natural period of the structure. One of the buildings reported values equal to 0.27s and 0.38s for a moderate damaged MIF structure.

Here, we remark that a proper estimation of the fundamental period is important to perform an adequate seismic evaluation of the structure, as it directly affects the estimation of expected deformation and, therefore, influences the damage forecast. In this particular case, considering the possibility that the fundamental period estimation of the blind-prediction model is low, results could lead to an underestimation of the seismic

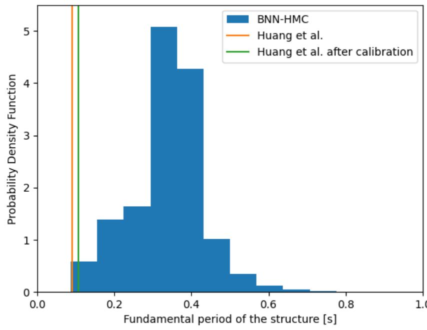

Figure 19: Predicted MIF fundamental period

effects. This study reflects that care must be taken when using deterministic models for prediction and it is strongly suggested that those models account for lower and upper bounds of the constitutive parameters or to complement the prediction with data measures taken from the real structure to be evaluated (for instance, ambient vibration of the structure).

5.2. Collapse evaluation by non-linear time history analysis

Non-linear time history analyses are performed using the blind-prediction, the calibrated and the data-based models presented in the previous section, along with FEMA-P695 far-field records.

According to ASCE 41 provisions, the deformation limit for collapse prevention performance criterion can be set from the point of maximum strength of the constitutive behaviour of a structural element, based on laboratory test results. Notice that current structural evaluation provisions define deformation capacities of the structural elements in a deterministic fashion, in terms of parameters that are subjected to uncertainties. These results makes evident that this approach can lead to biased results. Moreover, as shown in Figure 20, the blind-prediction model over-predicts the seismic capacity of the building, in comparison to the results obtained from the calibrated model (here assumed as the “true” result). This example shows the importance of obtaining reliable constitutive parameters for seismic evaluation of structures and demonstrates that a probabilistic data-based model, even with a high dispersion, can provide information more consistent with the expected behavior of an existing structure.

Figure 20 also shows the results obtained using the probabilistic approach with the model proposed in this work. Notice that the results from the calibrated model lay within the confidence interval of the proposed model prediction. Since the results obtained require minimal and easily available information, it can be considered that the proposed method constitutes a straightforward way of estimating the vulnerability of MIF buildings, being particularly suitable for macro-scale seismic vulnerability studies.

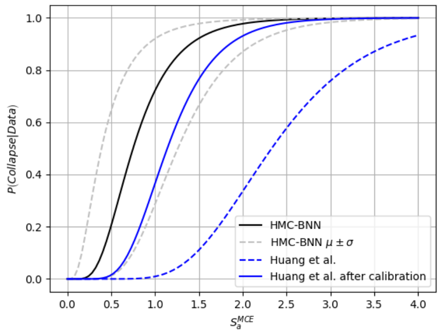

Figure 20: Comparison of fragility functions from the performed analyses.

6. Conclusions

This manuscript presented a new methodology for the probabilistic modelling and safety assessment of MIF buildings against lateral seismic loads. A simplified shear spring model to represent the in-plane behaviour of the MIF was proposed, where the parameters of the constitutive behaviour have been predicted by a HMC-BNN. The HMC-BNN model was trained with a number of available laboratory test results. The following conclusions arise from this investigation:

- Available data about the MIF structural system are scarce and, typically based on macro-scale structural, mechanical or geometrical features. Therefore, they are insufficient to properly develop precise micro-scale or meso-scale models. However, the model proposed herein helps to properly capture the expected in-plane lateral response of the MIF structures with quantified uncertainty, and without the need of numerous, yet typically unavailable, inputs.

- Considering all the sources of uncertainty that affect the seismic behavior of the MIFs, and after the results obtained in this work, the proposed methodology is recommended to enrich the existing deterministic models by accounting for the uncertainty in the estimates of the initial lateral stiffness, the maximum resistance, and the degradation of the structure, since these parameters have an important influence in the evaluation of the structural seismic safety.

- The proposed HMC-BNN model can be used at a macro-level approach to characterize the expected arquetype performance of groups of MIF buildings for risk evaluation. However, it also may be used as a first and rapid approach to estimate the expected behaviour of an existing structure, previous to a more in-depth structural evaluation.

Future research steps will aim to explore the application of physics-enriched neural networks to further exploit the predictive capabilities of micro or meso-models within the framework of artificial neural networks.

Acknowledgements

This work was supported by the SINDE (Research and Development System of the Catholic University of Santiago de Guayaquil, Ecuador) under project code 491/170, and by the Permanent Research Programme of Civil Engineering at University of Granada. The authors would also like to thank the TAQ-I-KISRA project funded by the National Research and Science Council of Spain under grant agreement No. RTI2018-101841-B-C21. The authors gratefully acknowledge the support of these organisations which have enabled the research reported in this paper.

Bibliography

[1] American Society of Civil Engineers (2016). *Minimum design loads for buildings and other structures (ASCE/SEI 7)*. ASCE, Reston, VA.

[2] Angel, R., Shapiro, D., Uzarski, J., and Webster, M. (1994). Behavior of Reinforced Concrete Frames With Masonry Infills. *Civil Engineering Studies*, 16509(589):183.

[3] ASCE/SEI 41 (2017). *Seismic Evaluation and Retrofit of Existing Buildings*. American Society of Civil Engineers, asce/sei 41-17 edition.

[4] Barbosa, A. R., Fahnestock, L. A., Fick, D. R., Gautam, D., Soti, R., Wood, R., Moaveni, B., Stavridis, A., Olsen, M. J., and Rodrigues, H. (2017). Performance of Medium-to-High Rise Reinforced Concrete Frame Buildings with Masonry Infill in the 2015 Gorkha, Nepal, Earthquake. *Earthquake Spectra*, 33(1, SI):S197–S218.

[5] Basha, S. H. and Kaushik, H. B. (2016). Behavior and failure mechanisms of masonry-infilled rc frames (in low-rise buildings) subject to lateral loading. *Engineering Structures*, 111:233–245.

[6] Benavent-Climent, A., Ramírez-Márquez, A., and Pujol, S. (2018). Seismic strengthening of low-rise reinforced concrete frame structures with masonry infill walls: Shaking-table test. *Engineering Structures*, 165:142–151.

[7] Benker, M., Furtner, L., Semm, T., and Zaeh, M. F. (2020). Utilizing uncertainty information in remaining useful life estimation via bayesian neural networks and hamiltonian monte carlo. *Journal of Manufacturing Systems*.

[8] Bennett, R. M., Flanagan, R. D., Adham, S., Fischer, W., and Tenbus, M. (1996). Evaluation and analysis of the performance of masonry infills during the northridge earthquake. Technical report, The National Science Foundation.

[9] Betancourt, M. (2017). A conceptual introduction to hamiltonian monte carlo. *arXiv preprint arXiv:1701.02434*.

[10] Blundell, C., Cornebise, J., Kavukcuoglu, K., and Wierstra, D. (2015). Weight uncertainty in neural network. In *International Conference on Machine Learning*, pages 1613–1622. PMLR.

[11] Bose, S., Martin, J., and Stavridis, A. (2019). Simulation framework for infilled RC frames subjected to seismic loads. *Earthquake Spectra*, 35(4):1739–1762.

[12] Calvi, G. M., Bolognini, D., and Penna, A. (2004). Seismic performance of masonry-infilled rc frames: benefits of slight reinforcements. *Invited lecture to "Sísmica*, 6:14–16.

[13] Cao, X.-Y., Feng, D.-C., and Beer, M. (2023). Consistent seismic hazard and fragility analysis considering combined capacity-demand uncertainties via probability density evolution method. *Structural Safety*, 103:102330.

[14] Chiozzi, A. and Miranda, E. (2017). Fragility functions for masonry infill walls with in-plane loading. *Earthquake Engineering and Structural Dynamics*, 46(15):2831–2850.

[15] Crisafulli, F. J. (1997). Seismic behaviour of reinforced concrete structures with masonry infills.

[16] Decanini, L. and Fantin, G. (1986). Modelos simplificados de la mampostería incluida en porticos. *Jornadas Argentinas de Ingeniería Estructural*, 2:817–836.

[17] Dhakal, R. and Maekawa, K. (2002). Modeling of post-yield buckling of reinforcement. *ASCE Journal of Structural Engineering*.

[18] Di Trapani, F., Macaluso, G., Cavaleri, L., and Papia, M. (2015). Masonry infills and RC frames interaction: Literature overview and state of the art of macromodeling approach. *European Journal of Environmental and Civil Engineering*, 19(9):1059–1095.

[19] EPN (2016). Observaciones del sismo del 16 de Abril de 2016 de Magnitud Mw 7.8. Intensidades y Aceleraciones. Technical Report 05, Instituto Geofísico. Escuela Politécnica Nacional.

[20] Feliciano, D., Arroyo, O., Carrillo, J., Liel, A. B., and Murray, P. B. (2023). Framework to assess the seismic performance of non-engineered masonry infilled RC frame buildings accounting for material uncertainty. *Structures*, 50(October 2022):1191–1203.

[21] Fernández, J., Chiachío, M., Chiachío, J., Muñoz, R., and Herrera, F. (2022). Uncertainty quantification in neural networks by approximate bayesian computation: Application to fatigue in composite materials. *Engineering Applications of Artificial Intelligence*, 107:104511.

[22] Fierro, E. A., Miranda, E., and Perry, C. L. (2011). *Behavior of Nonstructural Components in Recent Earthquakes*, chapter , pages 369–377. ASCE.

[23] Flanagan, R. D. and Bennett, R. M. (1999). In-plane behavior of structural clay tile infilled frames. *Journal of structural engineering*, 125(6):590–599.

[24] Furtado, A., Rodrigues, H., Arêde, A., and Varum, H. (2018). Double-leaf infill masonry walls cyclic in-plane behaviour: experimental and numerical investigation. *The Open Construction & Building Technology Journal*, 12(1).

[25] Gazić, G. and Sigmund, V. (2016). Cyclic testing of single-span weak frames with masonry infill. *Gradevinar*, 68(08):617–633.

[26] Ghahramani, Z. (2015). Probabilistic machine learning and artificial intelligence. *Nature*, 521(7553):452–459.

[27] Gilks, W., Richardson, S., and Spiegelhalter, D. (1996). *Markov chain Monte Carlo in practice*. Chapman and Hall/CRC, Boca Raton.

[28] Guerrero, N., Martinez, M., Picón, R., Marante, M. E., Hild, F., Roux, S., and Flórez-López, J. (2014). Experimental analysis of masonry infilled frames using digital image correlation. *Materials and structures*, 47(5):873–884.

[29] Haider, S. (1995). *In-plane cyclic response of reinforced concrete frames with unreinforced masonry infills*. PhD thesis, Rice University.

[30] Hak, S., Morandi, P., and Magenes, G. (2018). Prediction of inter-storey drifts for regular RC structures with masonry infills based on bare frame modelling. *Bulletin of Earthquake Engineering*, 16(1):397–425.

[31] Harris, J. R., Heintz, J. A., Manager, P., Hooper, J., Porush, A. R., Cranford, S., Haas, K., and Haselton, C. (2009). *Quantification of Building Seismic Performance Factors*. Federal Emergency Management Agency.

[32] Haselton, C. B., Liel, A., Taylor, S., and Deierlein, G. (2008). *Beam-column element model calibrated for predicting flexural response leading to global collapse of RC frame buildings*. Pacific Earthquake Engineering Research Center.

[33] Holmes, M. (1961). Steel frames with brickwork and concrete infilling. *proceedings of the Institution of civil Engineers*, 19(4):473–478.

[34] Huang, H., Burton, H. V., and Sattar, S. (2020). Development and Utilization of a Database of Infilled Frame Experiments for Numerical Modeling. *Journal of Structural Engineering (United States)*, 146(6).

[35] Irfanoglu, A. (2009). Performance of Template School Buildings during Earthquakes in Turkey and Peru. *Journal of Performance of Constructed Facilities*, 23(February):5–14.

[36] Jiang, H., Liu, X., and Mao, J. (2015). Full-scale experimental study on masonry infilled rc moment-resisting frames under cyclic loads. *Engineering Structures*, 91:70–84.

[37] Kallioras, S., Pohoryles, D. A., Bournas, D., Molina, F. J., and Pegon, P. (2023). Seismic performance of a full-scale five-story masonry-infilled RC building subjected to substructured pseudodynamic tests. *Earthquake Engineering and Structural Dynamics*, 52(12):3649–3678.

[38] Kalman Šipoš, T., Sigmund, V., and Hadzima-Nyarko, M. (2013). Earthquake performance of infilled frames using neural networks and experimental database. *Engineering Structures*, 51:113–127.

[39] Kam, W. Y., Pampanin, S., Dhakal, R., Gavin, H. P., and Roeder, C. (2010). Seismic performance of reinforced concrete buildings in the september 2010 Darfield (Canterbury) earthquake. *Bulletin of the New Zealand Society for Earthquake Engineering*, 43(4):340–350.

[40] Karthik, M. M. and Mander, J. B. (2011). Stress-block parameters for unconfined and confined concrete based on a unified stress-strain model. *Journal of Structural Engineering*, pages 270–273.

[41] Kaushik, H. B., Rai, D. C., and Jain, S. K. (2006). Code approaches to seismic design of masonry-infilled reinforced concrete frames: A state-of-the-art review. *Earthquake Spectra*, 22(4):961–983.

[42] Khansefid, A., Yadollahi, S. M., Taddei, F., and Müller, G. (2023). Fragility and comfortability curves development and seismic risk assessment of a masonry building under earthquakes induced by geothermal power plants operation. *Structural Safety*, 103:102343.

[43] Korkmaz, K. A., Kayhan, A. H., and Ucar, T. (2013). Seismic assessment of R/C residential buildings with infill walls in turkey. *Comp. Concrete*, 12(5):681–695.

[44] Liberatore, L., Noto, F., Mollaioli, F., and Franchin, P. (2018). In-plane response of masonry infill walls: Comprehensive experimentally-based equivalent strut model for deterministic and probabilistic analysis. *Engineering Structures*, 167:533–548.

[45] Maidiawati and Sanada, Y. (2017). R/C frame-infill interaction model and its application to Indonesian buildings. *Earthquake Engineering & Structural Dynamics*, 46(2):221–241.

[46] Mansouri, A., Marefat, M. S., and Khanmohammadi, M. (2014). Experimental evaluation of seismic performance of low-shear strength masonry infills with openings in reinforced concrete frames with deficient seismic details. *The Structural Design of Tall and Special Buildings*, 23(15):1190–1210.

[47] Markulak, D., Radić, I., and Sigmund, V. (2013). Cyclic testing of single bay steel frames with various types of masonry infill. *Engineering structures*, 51:267–277.

[48] Mehrabi, A. B., Benson Shing, P., Schuller, M. P., and Noland, J. L. (1996). Experimental evaluation of masonry-infilled rc frames. *Journal of Structural engineering*, 122(3):228–237.

[49] Mohamed, H. and Romão, X. (2018). Robust Calibration of Macro-Models for the In-Plane Behavior of Masonry Infilled RC Frames. *Journal of Earthquake Engineering*, 00(00):1–27.

[50] Mohammad Noh, N., Liberatore, L., Mollaioli, F., and Tesfamariam, S. (2017). Modelling of masonry infilled RC frames subjected to cyclic loads: State of the art review and modelling with OpenSees. *Engineering Structures*, 150:599–621.

[51] Morandi, P., Hak, S., and Magenes, G. (2018a). Mechanical characterization and force-displacement hysteretic curves from in-plane cyclic tests on strong masonry infills. *Data in Brief*, 16:886 – 904.

[52] Morandi, P., Hak, S., and Magenes, G. (2018b). Performance-based interpretation of in-plane cyclic tests on RC frames with strong masonry infills. *Engineering Structures*, 156:503–521.

[53] Neal, R. (1996). *Bayesian Learning for Neural Networks*. Lecture Notes in Statistics. Springer New York.

[54] Neal, R. M. (1993). Probabilistic inference using markov chain monte carlo methods. Technical Report CRG-TR-93-1, Department of computer science. University of Toronto.

[55] O'Reilly, G. J., Perrone, D., Fox, M., Monteiro, R., and Filiatrault, A. (2018). Seismic assessment and loss estimation of existing school buildings in Italy. *Engineering Structures*, 168(April):142–162.

[56] Panagiotakos, T. B. and Fardis, M. N. (2001). Deformations of reinforced concrete members at yielding and ultimate. *Structural Journal*, 98(2):135–148.
[57] Perrone, D., Calvi, P. M., Nascimbene, R., Fischer, E. C., and Magliulo, G. (2018). Seismic performance of non-structural elements during the 2016 Central Italy earthquake. *Bulletin of Earthquake Engineering*.
[58] Pujol, S. and Fick, D. (2010). The test of a full-scale three-story RC structure with masonry infill walls. *Engineering Structures*, 32(10):3112–3121.
[59] Rahbar, E., Permanoon, A., and Akhaveissy, A. H. (2023). Numerical evaluation of masonry-infill frames: Analysis of lateral strength and failure modes on meso scale. *Structures*, 52:779–793.
[60] Sattar, S. and Liel, A. B. (2016a). Seismic performance of nonductile reinforced concrete frames with masonry infill walls - II: Collapse assessment. *Earthquake Spectra*, 32(2):819–842.
[61] Sattar, S. and Liel, A. B. (2016b). Seismic performance of nonductile reinforced concrete frames with masonry infill walls—I: development of a strut model enhanced by finite element models. *Earthquake Spectra*, 32(2):795–818.
[62] Sayin, E. and Calayir, Y. (2015). Comparison of linear and non-linear earthquake response of masonry walls. *Comp. Concrete*, 16(1):17–35.
[63] Schneider, S. P., Zagers, B. R., and Abrams, D. P. (1998). Lateral strength of steel frames with masonry infills having large openings. *Journal of Structural Engineering*, 124(8):896–904.
[64] Sigmund, V. and Penava, D. (2014). Influence of openings, with and without confinement, on cyclic response of infilled rc frames—an experimental study. *Journal of earthquake engineering*, 18(1):113–146.
[65] Stafford Smith, B. and Carter, C. (1969). A method of analysis for infilled frames. *Proceedings of the institution of civil engineers*, 44(1):31–48.
[66] Stavridis, A., Koutromanos, I., and Shing, P. B. (2012). Shake-table tests of a three-story reinforced concrete frame with masonry infill walls. *Earthquake Engineering and Structural Dynamics*, 41(6):1089–1108.
[67] Tarque, N., Candido, L., Camata, G., and Spacone, E. (2015). Masonry infilled frame structures: state-of-the-art review of numerical modelling. *Earthquakes and Structures*, 8(3):733–759.
[68] Tasnimi, A. A. and Mohebkhah, A. (2011). Investigation on the behavior of brick-infilled steel frames with openings, experimental and analytical approaches. *Engineering Structures*, 33(3):968–980.
[69] Urich, A. J. and Beauperthuy, J. L. (2012). Protagonism of the Infill Walls on Seismic Performance of Venezuela Buildings. *15th World Conference on Earthquake Engineering (15WCEE)*.
[70] Varum, H., Furtado, A., Rodrigues, H., Dias-Oliveira, J., Vila-Pouca, N., and Arêde, A. (2017). Seismic performance of the infill masonry walls and ambient vibration tests after the Ghorka 2015, Nepal earthquake. *Bulletin of Earthquake Engineering*, 15(3):1185–1212.
[71] Villalobos, E., Sim, C., Smith-Pardo, J. P., Rojas, P., Pujol, S., and Kreger, M. E. (2018). The 16 April 2016 Ecuador earthquake damage assessment survey. *Earthquake Spectra*, 34(3):1201–1217.
[72] Zhu, M., McKenna, F., and Scott, M. H. (2018). Openseespy: Python library for the opensees finite element framework. *SoftwareX*, 7:6–11.

Appendix 1

This section specifies the data of the cyclic lateral in-plane tests used in this work. Figure 5 depicts the meaning of the parameters of the tables.

Table 7: Data of masonry infilled steel frame tests (Units: mm, MPa).

Author	No.	Unit[a]	$\frac{h_m}{t_m}$[b]	$\frac{h_m}{L_m}$	λ	$\frac{P}{A_m f_m}$[c]	A_{is}^r[d]	A_{is}^l	Δ_y^+	Δ_y^-	Δ_c^+	Δ_c^-	Δ_{85}^+	Δ_{85}^-	V_y^+	V_y^-	V_c^+	V_c^-	V_{85}^+	V_{85}^-
Flanagan 1994	1	HCl	11.49	1.00	9.74	0.00%	2.79	2.79	7.92	8.96	19.73	27.94	19.98	29.58	59.30	87.09	160.28	124.41	133.86	91.98
	2	HCl	11.49	1.00	5.86	0.00%	2.79	2.79	13.38	13.44	25.91	27.24	26.15	30.40	115.34	105.80	181.64	167.94	149.37	108.27
	3	HCl	11.49	1.00	4.38	0.00%	2.79	2.79	7.03	10.10	12.91	14.59	15.00	17.34	111.57	93.13	172.98	151.69	134.16	106.04
	4	HCl	6.79	1.00	8.10	0.00%	2.79	2.79	7.55	11.99	14.11	13.31	20.02	25.74	92.15	158.58	147.68	229.49	55.19	76.36
	5	HCl	6.79	1.00	6.15	0.00%	2.79	2.79	5.22	6.35	14.11	13.31	17.19	18.94	114.54	137.20	167.46	196.01	116.49	165.63
	6	HCl	18.82	1.00	5.18	0.00%	2.79	2.79	5.22	6.35	14.11	13.31	17.19	18.94	114.54	137.20	167.46	196.01	116.49	165.63
	7	HCl	11.49	1.00	3.28	0.00%	2.79	2.79	5.03	6.61	10.85	11.05	15.19	14.60	121.17	156.78	211.83	223.97	157.45	170.66
	8	HCl	11.49	0.79	5.82	0.00%	3.61	3.61	34.94	32.09	46.78	50.11	46.78	51.70	94.84	141.74	141.76	205.42	141.76	174.59
	9	HCl	11.49	0.79	5.82	0.00%	3.61	3.61	10.82	13.03	22.79	27.03	23.11	29.24	108.10	85.88	155.99	148.58	116.79	83.80
	10	HCl	11.49	0.65	5.73	0.00%	4.61	4.61	30.16	10.84	63.98	28.34	63.98	46.24	142.04	111.41	205.26	198.95	205.26	48.48
	11	HCl	11.49	0.79	5.82	0.00%	3.61	3.61	15.99	19.79	32.90	38.09	37.94	40.72	130.99	124.12	202.14	177.32	69.32	150.23
	12	HCl	11.49	0.79	5.82	0.00%	3.61	3.61	10.13	22.08	31.43	36.37	36.89	36.89	55.94	103.56	146.44	171.45	124.38	126.46
	13	HCl	11.49	0.79	5.82	0.00%	3.61	3.25	10.62	12.90	16.00	18.79	16.41	18.97	90.57	42.33	134.18	66.98	79.36	23.15
Markulak, Radic, Vladimir 2013	14	AAC	12.45	0.76	4.89	0.00%	1.84	1.84	10.58	5.48	29.98	13.72	30.54	13.72	90.64	69.93	138.59	99.90	108.92	99.90
	15	HCl	12.45	0.76	3.20	0.00%	1.84	1.84	5.36	4.20	15.59	16.86	15.59	18.19	95.17	95.20	135.95	136.00	105.83	128.81
	16	AAC	12.45	0.76	4.96	0.00%	1.84	1.84	3.66	3.39	15.22	13.22	15.43	13.22	76.39	62.10	109.13	88.72	105.66	88.72
	17	AAC	12.45	0.76	4.96	0.00%	1.84	1.84	3.54	3.01	16.36	7.94	17.00	8.18	63.42	58.63	90.60	83.76	86.32	79.49
	18	AAC	12.45	0.76	4.96	0.00%	1.84	1.84	5.47	4.08	16.99	13.17	17.08	13.26	66.46	56.41	94.94	80.59	91.56	76.37
Schneider, Zagers, Abrams 1998	19	SCl	22.16	0.73	2.88	0.21%	1.40	1.40	5.19	10.80	16.53	24.05	26.00	25.66	29.77	51.74	65.86	82.79	55.48	70.34
	20	SCl	11.08	0.73	3.66	1.00%	1.40	1.40	11.57	4.68	23.76	22.03	39.07	34.07	122.76	79.11	180.26	177.78	141.80	149.55
	21	SCl	22.16	0.73	3.12	1.63%	1.65	1.65	6.59	8.57	13.62	20.29	26.39	25.88	79.91	87.80	125.06	125.42	103.26	105.84
	22	SCl	11.08	0.73	3.68	1.80%	1.65	1.65	8.62	12.34	20.64	32.69	29.12	41.14	133.09	133.97	196.89	194.72	167.10	128.69
	23	SCl	22.16	0.73	3.03	2.03%	1.96	1.96	8.62	12.34	13.57	20.19	29.12	41.14	133.09	133.97	196.89	194.72	167.10	128.69
Tasmini, Mohe-bkhah 2011	24	SCl	16.36	0.80	5.23	0.00%	2.31	2.31	8.14	6.27	20.00	20.00	50.20	45.39	141.76	151.03	202.51	215.75	166.98	183.36
	25	SCl	16.36	0.80	5.23	0.00%	2.06	2.06	4.11	3.46	15.25	14.59	39.12	24.91	122.05	123.49	174.36	176.41	147.56	149.55
	26	SCl	16.36	0.80	5.16	0.00%	1.78	1.78	3.89	2.83	13.80	13.53	33.91	30.05	106.76	96.28	152.52	137.54	118.83	103.86
	27	SCl	16.36	0.80	5.16	0.00%	1.63	1.63	4.56	4.12	14.93	25.00	34.74	45.58	96.34	86.32	137.63	123.32	116.23	104.77
	28	SCl	16.36	0.80	5.41	0.00%	1.51	1.51	3.91	5.88	13.95	29.75	44.79	41.18	82.17	87.88	117.39	125.54	98.23	97.83

[a] Masonry Unit types: SC: Solid Concrete, HC: Hollow Concrete, FA: Fly Ash, SCl: Solid Clay, HCl: Hollow Clay, AAC: Autoclaved Aerated Concrete

[b] h_m, t_m and L_m are the height, thickness and length of the masonry infill in [mm], respectively

[c] P is the axial load acting on the wall, $A_m = L_m t_m$ and f_m is the characteristic axial strength of the masonry wall.

[d] Area of the equivalent strut according to Holmes [33] considering windows and doors openings, in m^2.

Table 8: Data of masonry infilled reinforced concrete frame tests (Units: mm, MPa).

Author	No.	Unit[a]	$\frac{h_m}{t_m}$[b]	$\frac{h_m}{L_m}$	λ	$\frac{P}{A_m f_m}$[c]	A_{is}^r[d]	A_{is}^l	Δ_y^+	Δ_y^-	Δ_c^+	Δ_c^-	Δ_{85}^+	Δ_{85}^-	V_y^+	V_y^-	V_c^+	V_c^-	V_{85}^+	V_{85}^-
Morandi et al., 2018	29	HCl	8.43	0.70	4.49	11.67%	7.27	7.27	12.83	12.16	45.55	44.29	47.43	46.18	395.31	414.91	564.72	592.73	508.70	570.35
	30	HCl	8.43	0.70	4.49	11.67%	7.27	7.27	10.63	10.45	46.17	46.51	62.31	78.04	382.95	388.56	547.07	555.09	456.04	453.71
	31	HCl	8.43	0.70	4.49	11.67%	7.27	7.27	8.25	11.42	28.40	30.23	29.62	30.23	329.82	333.55	471.17	476.50	365.48	476.50
	32	HCl	8.43	0.70	4.49	11.67%	4.26	4.26	8.93	6.02	31.04	31.04	31.29	31.16	203.56	207.82	290.80	296.88	264.01	273.96
Basha y Kaushik, 2016	33	FA	13.64	1.00	4.01	1.40%	1.25	1.25	2.42	1.79	11.71	13.50	36.01	26.90	45.32	43.03	64.74	61.48	54.95	52.05
	34	FA	13.64	1.00	4.01	1.40%	1.25	1.25	3.24	4.92	12.09	12.98	30.90	26.41	54.46	57.65	77.80	85.41	65.83	69.09
	35	FA	13.64	1.00	4.01	1.40%	1.25	1.25	1.49	2.35	30.54	31.30	57.71	45.38	44.60	49.13	63.72	70.19	48.81	59.50
	36	FA	13.64	1.00	4.01	1.40%	1.25	1.25	4.50	6.00	13.50	18.90	45.90	27.10	65.31	61.77	99.10	88.25	79.71	74.64
	37	FA	27.27	1.00	3.37	2.80%	1.25	1.25	1.43	3.30	10.81	15.30	35.11	31.50	62.80	47.61	89.72	68.01	65.61	56.99
	38	FA	27.27	1.00	3.37	2.80%	1.25	1.25	1.81	2.99	10.80	9.90	31.50	31.49	52.06	45.57	74.38	70.00	60.16	59.06
Calvi, Bolognini y Penna, 2004	39	HCl	23.91	0.65	2.94	0.00%	6.87	6.87	11.50	7.19	12.00	9.39	12.08	18.26	168.16	124.70	240.22	205.44	120.58	205.44
	40	HCl	23.91	0.65	2.94	0.00%	6.87	6.87	10.78	6.01	10.60	12.17	106.78	21.42	170.78	131.80	243.98	298.19	236.75	252.24
	41	HCl	23.91	0.65	2.94	0.00%	6.87	6.87	5.80	11.79	11.10	12.00	11.85	107.61	132.21	204.56	252.79	292.23	129.18	234.09
	42	HCl	20.37	0.65	3.06	0.00%	6.87	6.87	3.83	7.30	7.30	5.22	10.78	5.42	207.00	121.34	300.00	366.58	232.14	97.45
	43	HCl	23.91	0.65	2.94	0.00%	6.87	6.87	1.97	2.54	4.70	5.64	8.89	9.14	180.00	160.00	257.14	228.57	192.86	117.13
	44	HCl	23.91	0.65	2.94	0.00%	6.87	6.87	2.29	2.15	5.35	6.03	8.97	8.62	158.12	195.47	225.89	279.25	172.53	236.56
	45	HCl	20.37	0.65	3.06	0.00%	6.87	6.87	3.47	2.23	9.14	5.61	9.17	9.22	185.44	213.39	264.92	304.84	212.90	229.72
Gazic y Sigmund, 2016	46	HCl	14.44	0.70	5.18	66.07%	1.40	1.40	1.89	2.24	4.27	3.59	5.54	5.13	110.67	89.69	158.10	137.14	132.25	114.67
	47	HCl	14.44	0.70	5.18	66.07%	1.40	1.40	1.58	2.27	3.85	4.08	5.48	5.58	116.93	94.94	168.00	138.00	136.00	115.33
	48	SCl	20.00	0.70	4.78	80.92%	1.40	1.40	2.31	1.77	21.93	12.76	24.42	24.42	139.76	111.62	199.66	159.46	175.68	113.59
	49	HCl	14.44	0.70	3.53	150.15%	1.40	1.40	0.39	0.70	6.10	2.82	8.76	11.73	54.91	53.57	78.44	76.52	65.43	56.15
	50	SCl	20.00	0.70	3.20	120.23%	1.40	1.40	0.70	0.54	15.43	2.25	21.51	24.28	30.45	23.49	43.50	34.50	33.40	28.00
	51	HCl	14.44	0.70	5.18	66.07%	1.40	1.40	6.10	5.75	22.13	18.06	22.38	24.39	41.36	40.42	61.82	57.74	50.69	50.58
	52	SCl	20.00	0.70	3.21	80.92%	1.40	1.40	1.93	1.69	5.85	13.35	6.32	14.79	116.94	118.59	167.06	169.41	135.29	141.65
	53	HCl	14.44	0.74	3.55	69.84%	1.40	1.40	1.89	2.05	10.45	5.23	12.05	12.95	154.65	145.20	220.93	218.02	186.05	177.33
	54	SCl	20.00	0.74	2.19	85.55%	1.40	1.40	3.30	2.80	10.36	17.50	10.36	18.90	208.47	202.26	297.82	288.94	235.60	280.61
Guerrero et al., 2014	55	HC	10.33	0.65	3.88	0.00%	2.22	2.22	9.04	7.52	23.85	22.81	44.59	44.50	95.72	82.96	136.74	118.51	111.88	100.58
	56	HC	12.00	0.75	4.40	0.00%	2.48	2.48	5.07	4.81	19.00	52.00	55.80	93.95	33.95	29.05	48.50	41.50	41.20	35.26
	57	HC	12.00	0.75	4.40	0.00%	2.48	2.48	6.58	0.55	15.34	0.55	39.52	0.55	81.34	0.00	116.20	0.00	98.62	0.00

[a] Masonry Unit types: SC: Solid Concrete, HC: Hollow Concrete, FA: Fly Ash, SCl: Solid Clay, HCl: Hollow Clay, AAC: Autoclaved Aerated Concrete

[b] h_m, t_m and L_m are the height, thickness and length of the masonry infill in [mm], respectively

[c] P is the axial load acting on the wall, $A_m = L_m t_m$ and f_m is the characteristic axial strength of the masonry wall.

[d] Area of the equivalent strut according to Holmes [33] considering windows and doors openings, in m^2.

Table 9: Data of masonry infilled reinforced concrete frame tests (Units: mm, MPa).

Author	No.	Unit[a]	$\frac{h_m}{t_m}$[b]	$\frac{h_m}{L_m}$	λ	$\frac{P}{A_m f_m}$[c]	A_{is}^r[d]	A_{is}^l	Δ_y^+	Δ_y^-	Δ_c^+	Δ_c^-	Δ_{85}^+	Δ_{85}^-	V_y^+	V_y^-	V_c^+	V_c^-	V_{85}^+	V_{85}^-
Haider, 1995	58	SCl	23.26	1.09	2.80	0.00%	2.20	2.20	9.82	9.81	20.11	20.09	40.96	35.96	138.08	151.16	216.43	221.64	177.70	188.04
	59	SCl	23.26	1.09	2.31	0.00%	2.20	2.20	12.77	17.37	30.01	34.97	71.21	62.23	169.76	193.22	242.52	289.68	172.57	246.15
	60	SCl	23.26	1.09	3.00	0.00%	2.20	2.20	13.86	6.45	29.78	25.75	29.78	25.76	95.11	69.14	136.06	188.39	130.83	177.93
	61	SCl	23.26	1.09	2.49	0.00%	2.20	2.20	12.19	14.65	30.30	30.74	40.67	61.70	149.43	188.09	213.47	268.69	149.82	224.49
Jiang, Liu y Mao, 2015	62	AAC	13.63	0.49	4.00	31.39%	10.03	10.03	3.70	6.14	40.71	43.93	64.29	65.55	409.69	466.38	585.28	666.26	496.93	566.09
	63	AAC	13.63	0.49	4.00	31.39%	10.03	10.03	21.49	24.36	54.16	73.27	76.46	99.82	343.17	311.88	490.24	468.29	402.44	431.71
	64	AAC	13.63	0.49	4.00	31.39%	10.03	10.03	21.49	24.36	54.16	73.27	76.46	99.82	343.17	311.88	490.24	468.29	402.44	431.71
	65	AAC	13.63	0.49	4.00	31.39%	10.03	10.03	18.71	14.53	48.97	53.27	51.12	58.65	354.20	288.44	511.11	488.89	414.82	385.19
	66	AAC	13.63	0.49	4.00	31.39%	10.03	10.03	15.00	17.14	63.21	45.00	101.79	79.29	299.54	248.40	490.24	504.88	402.44	428.05
	67	AAC	13.63	0.49	4.00	31.39%	10.03	10.03	20.35	16.53	80.54	74.13	100.80	107.20	312.44	292.50	446.34	475.61	343.90	402.44
Mansouri et al., 2014	68	SCl	12.26	0.62	1.77	30.47%	1.65	1.65	16.11	17.18	43.53	51.72	45.15	57.97	79.23	81.14	113.18	115.91	69.33	79.09
	69	SCl	12.26	0.62	1.77	30.47%	1.39	1.26	14.46	12.43	58.01	27.21	58.01	45.53	53.30	57.77	76.15	83.49	76.15	65.14
	70	SCl	12.26	0.62	1.77	30.47%	1.25	1.25	11.99	10.82	28.70	27.91	45.49	44.72	62.94	62.29	89.91	88.99	57.06	46.90
	71	SCl	12.26	0.62	1.77	30.47%	1.21	1.41	10.86	8.42	34.21	17.19	35.31	33.01	58.57	63.81	83.67	92.48	63.34	78.55
Mehrabi, Shing, Schuller y Noland, 1996	72	HC	15.43	0.67	3.95	0.01%	1.79	1.79	1.61	2.50	11.76	10.32	20.04	16.90	111.73	104.72	159.61	149.59	135.29	125.17
	73	SC	15.43	0.48	4.50	0.01%	2.81	2.81	1.48	1.27	5.28	8.12	17.26	9.45	176.13	194.57	287.80	277.96	238.60	230.95
	74	HC	15.43	0.67	3.26	0.01%	1.79	1.79	3.04	1.69	9.85	4.38	10.19	12.94	144.22	127.23	206.03	181.76	140.09	132.05
	75	SC	15.43	0.67	4.61	0.01%	1.79	1.79	1.70	0.84	8.75	15.51	20.05	19.18	184.72	156.76	263.89	223.94	223.66	184.18
	76	SC	15.43	0.48	4.10	0.00%	2.81	2.81	0.95	2.06	6.78	8.18	7.15	17.53	252.88	242.35	361.26	346.21	306.36	293.99
	77	SC	15.43	0.67	4.44	0.01%	1.79	1.79	2.34	3.94	8.38	9.72	12.23	9.76	304.97	310.14	443.27	487.64	375.72	367.11
Sigmund y Penava (2014)	78	HCl	10.83	0.72	2.87	62.59%	1.11	1.11	1.10	1.25	6.06	4.55	6.06	5.02	160.69	172.51	257.93	246.45	257.93	183.88
	79	HCl	10.83	0.72	3.01	62.59%	1.06	1.06	1.65	1.29	6.45	4.62	7.20	4.68	209.44	183.45	299.19	290.73	245.57	224.75
	80	HCl	10.83	0.72	2.93	62.59%	1.08	1.22	1.49	1.64	8.26	10.08	13.27	10.54	194.60	182.73	278.00	261.05	184.44	255.39
	81	HCl	10.83	0.72	2.89	62.59%	1.14	1.10	1.89	1.01	14.38	13.02	17.99	13.17	208.97	153.37	298.53	219.11	242.09	202.11
	82	HCl	10.83	0.72	2.95	62.59%	1.11	1.11	1.89	1.52	4.72	4.87	10.58	5.70	216.89	194.80	309.84	278.28	261.07	195.30
	83	HCl	10.83	0.72	2.95	62.59%	1.06	1.06	1.19	2.48	7.99	6.29	13.52	14.89	180.74	214.88	258.20	306.97	220.90	261.07
	84	HCl	10.83	0.72	2.93	62.59%	1.08	1.22	1.27	1.48	13.81	9.07	14.11	12.73	197.00	193.00	281.43	275.71	281.43	261.43
	85	HCl	10.83	0.72	3.05	62.59%	1.35	1.35	1.40	0.90	4.20	3.07	4.64	3.10	195.84	123.24	279.77	275.08	138.13	158.91

[a] Masonry Unit types: SC: Solid Concrete, HC: Hollow Concrete, FA: Fly Ash, SCl: Solid Clay, HCl: Hollow Clay, AAC: Autoclaved Aerated Concrete

[b] h_m, t_m and L_m are the height, thickness and length of the masonry infill in [mm], respectively

[c] P is the axial load acting on the wall, $A_m = L_m t_m$ and f_m is the characteristic axial strength of the masonry wall.

[d] Area of the equivalent strut according to Holmes [33] considering windows and doors openings, in m^2.